Macromolecules

Cite This: Macromolecules 2019, 52, 332−340

Article

pubs.acs.org/Macromolecules

Peculiar Aggregation Features in Poly(3-hexylthiophene)/Chlorobenzene Solutions

Han-Liou Yi and Chi-Chung Hua*

Department of Chemical Engineering, National Chung Cheng University, Chiayi 62102, Taiwan

Supporting Information

ABSTRACT: We report on anomalous structure and relaxation features of the aggregate clusters fostered in a representative series of dilute poly(3-hexylthiophene)/chlorobenzene (P3HT/CB) solutions (3, 5, 8, and 10 mg/mL), as resolved by multiscale dynamic/static analysis schemes including depolarized/polarized dynamic light scattering (DDLS/DLS), static light/X-ray scattering (SALS/SLS/SAXS), and scanning transmission electron/transmission electron microscopy (STEM/TEM). DLS/DDLS analyses reveal the coexistence and dynamic equilibrium of diffusive isolated-chain species (fast mode) and *nondiffusive*, microsized cluster species (slow mode), largely unaffected by the polymer concentration, system temperature, sonication, laser exposure time, and, in particular, repeated filtrations during the sample preparation and measurements. The SALS/SLS/SAXS analyses further reveal that while the fast mode corresponds to isolated chains (R_g ∼ 1.5 nm), the slow mode represents microsized clusters comprising a condensed core (R_g ∼ 4 μm) and loose corona (∼700 nm in shell thickness). These combined features and detailed analyses performed herein suggest that the core−shell cluster—which is rarely observed for homopolymer solutions—is formed during a dynamic equilibrium process wherein the isolated chains undergo condensation/decomposition on the (stabilized) core material, leading to an apparent "elastic" slow-mode relaxation whose apparent rate is set by the core-material diffusion. Only at a low temperature (15 °C) and high concentration (c > 5 mg/mL) does the shell material become indistinguishable from the core material, when one has a homogeneous and fairly condensed cluster that exhibits the normal diffusional behavior. The present findings provide new insight into the mechanistic aspects and precise controls of the morphological properties of P3HT solutions for future applications with polymer-based electronic devices.

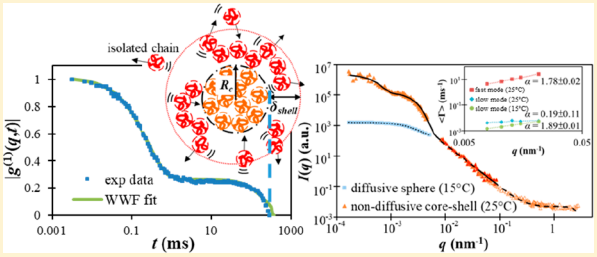

1. INTRODUCTION

Since the discovery of highly conductive polyacetylene by Shirakawa[1,2] about four decades ago, conducting conjugated polymers have continued to attract much attention nowadays because of their remarkable optoelectronic properties combined with low cost and large-area solution processability as well as device flexibility.[3] Poly(3-hexylthiophene) (P3HT)[4,5] is among the frontrunners of its kind due to its ease of synthesis and good optoelectronic properties for a broad range of applications with organic photovoltaic devices (OPVs), organic light-emitting diodes (OLEDs), and organic thin-film transistors (OTFTs). According to the current literature, however, the performance of P3HT-based devices can vary substantially, depending on a number of sample preparation and processing conditions.[4,6−8] Early research has demonstrated, in particular, that the aggregation state in P3HT films has an important influence on the mobility of charge carriers,[6,9,10] which in turn is strongly correlated to the polymer morphologies formed first in solution and later during thin-film fabrication.[7,11,12] Although the highest values of charge carrier mobility in OTFTs have so far been reported for P3HT films bearing an expanded nanofibril (semicrystalline) network,[7,13,14] other varieties of aggregate morphologies are possible in P3HT films[13,15−20] whose applications are yet to be fully explored.

A common strategy to manipulate the thin-film morphologies of a conjugated polymer is through controlling the molecular properties or chain interactions in the pristine solution with varying polymer concentration and solvent medium. For P3HT solutions, early studies have revealed two ubiquitous molecular species in dynamic light scattering (DLS) and UV−vis absorption analyses,[15,18,21−23] namely, isolated chains and large aggregates. The second (aggregate) species is of particular interest because it may serve as a supramolecular bridge or seed particle to enhance local electron conduction in thin film, while still larger (microsized) clusters may be fostered in solution as well by adding poor or non-solvents[6,7,9−11] that, in turn, can substantially promote mesoscale charge transfers. Thus, understanding the (dynamic and static) attributes of the aggregate species in solution is crucial for precise controls over the thin-film morphology and device performance.

In this study focusing on a series of dilute P3HT/CB (chlorobenzene) solutions, the DLS analysis first reveals the

Received: December 10, 2018
Published: December 21, 2018

Downloaded via SYNCHROTRON RADIATION RESEARCH on January 10, 2020 at 08:00:08 (UTC).
See https://pubs.acs.org/sharingguidelines for options on how to legitimately share published articles.

© 2018 American Chemical Society

DOI: 10.1021/acs.macromol.8b02619
Macromolecules 2019, 52, 332−340

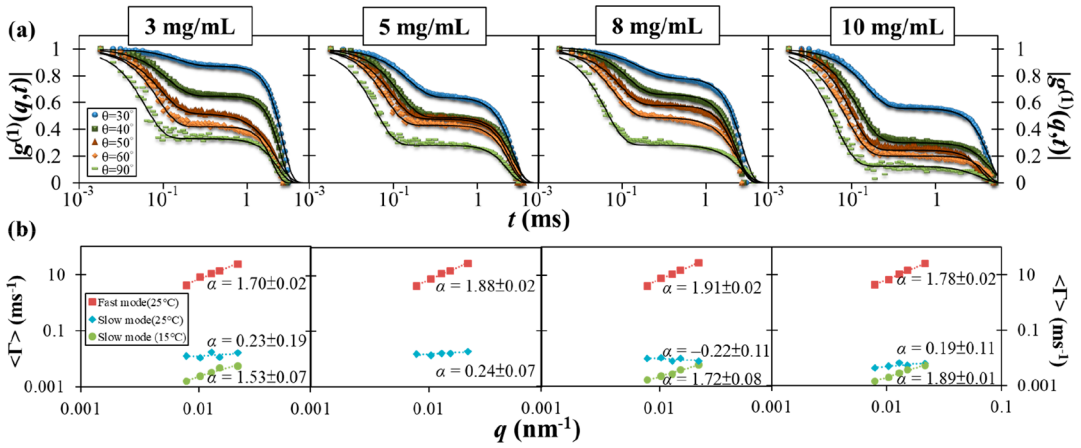

Figure 1. Concentration dependences of (a) the field autocorrelation function, $|g^{(1)}(q,t)|$, and (b) the associated decay rate, $\langle\Gamma\rangle$, as a function of the scattering vector q, $\langle\Gamma\rangle \sim q^{\alpha}$, for four P3HT/CB solutions at 25 °C. The data in (a) are fitted using eq 1 (solid lines). For comparison, the results for a lower temperature 15 °C (green symbols) are also shown in (b) for the slow mode.

coexistence of two distinct species. A detailed (multiangular) analysis, however, indicates that only the first (fast) mode bears the usual diffusive attribute that allows for an unambiguous determination of its hydrodynamic size. The second (slow) mode, whose attributes have acquired little or no systematic exploration in previous work, demonstrates a peculiarly nondiffusive relaxation and therefore prevents a direct assessment of its hydrodynamic size and structural features. Observing further that this essential slow-mode relaxation seems unaffected by a number of experimental factors investigated herein, its ubiquity may be inferred, and further structural analyses are performed using multiscale static light/X-ray scattering and electron microscopy (EM) characterization schemes. The results provide compelling evidence that the "elastic" microsized clusters identified for P3HT/CB solutions bear a core−shell structure, which is suggested to be formed during a dynamic equilibrium process wherein the isolated chains undergo condensation/decomposition on the (stabilized) core material. As similar core−shell clusters have rarely been reported for P3HT solutions in particular and homopolymer solutions in general, the overall findings provide new insight into the mechanistic aspects and precise controls of the morphological properties of P3HT solutions for future applications with polymer-based electronic devices.

2. EXPERIMENTAL METHODS

2.1. Materials and Sample Preparation. The regioregular P3HT sample investigated herein (average molecular weight M_w = 48105 g/mol, polydispersity index PDI = 2.27, regioregularity >95%) was purchased from Luminescence Technology Corp. (Taiwan) and used without further purification. The solvent used to dissolve P3HT, CB (Sigma-Aldrich, USA, ≥99.5% in purity), was filtered through a 0.22 μm PVDF filter (Millipore Millex-GN) to remove dust. Unless otherwise stated, dilute P3HT/CB solutions (3, 5, 8, and 10 mg/mL; the intrinsic viscosity analyses shown in Figure S1 (Supporting Information) led to an estimated overlap concentration of $c^* \sim 12$ mg/mL) were sonicated for 2 h at 70.0 °C to expedite the dissolution process, whereby transparent and homogeneous solutions were obtained. The resulting solution was further filtered into dust-free vial using 0.45 μm PVDF filter and was allowed to equilibrate for at least 1 h at room temperature before being transferred to the sample carriers for all subsequent characterizations.

2.2. Light Scattering (SLS/DLS/DDLS) Analyses. Light scattering (LS) measurements were performed on a laboratory-built apparatus as described elsewhere.[24,25] A 18 mW polarized He−Ne laser (λ_0 = 632.8 nm; Lasos, LGK 7665 P18) was used as the incident light, at which the investigated P3HT solutions show negligible absorption (Figure S2). Unless otherwise stated, all measurements were conducted at 25.0 ± 0.1 °C for a range of scattering angles θ = 30°−140°. Detailed descriptions of the static, dynamic, and depolarized dynamic light scattering (SLS/DLS/DDLS) analysis schemes can be found in prior work.[26,27]

2.3. Small-Angle Light/X-ray Scattering (SALS/SAXS) Analyses. The apparatus for SALS measurements was described elsewhere.[25] A 2 mW He−Ne laser with a wavelength of λ_0 (= 632.8 nm) was used as the incident light, and data were collected in a range of scattering angles θ = 0.7°−20°. SAXS measurements were performed at beamline stations BL23A of the Taiwan Light Source (TLS) and BL25A of the Taiwan Photon Source (TPS) at the National Synchrotron Radiation Research Center (NSRRC) in Taiwan. For the TLS facility, the scattering X-ray covers a q-range of 0.04−3.0 nm^{-1}, with 15 keV incident beam (wavelength λ_0 = 0.827 Å) and sample-to-detector distance of 4714 mm; for the TPS facility, the scattering X-ray covers a q-range of 0.01−1.0 nm^{-1}, with 8.827 keV incident beam (wavelength λ_0 = 1.405 Å) and sample-to-detector distance of 10.08 m. All measurements were conducted at 25.0 ± 0.1 °C.

2.4. Electron Microscopy (EM) Analyses. The EM images were taken from the transmission electron microscope (JEOL JEM-2010) at an acceleration voltage of 200 kV as well as from the scanning transmission electron microscope (Hitachi S4800-I) at an acceleration voltage of 15 kV. The sample solution was filtered through a copper grid coated with carbon film, which was placed on a filter paper (ADVANTEC filter paper 1) to undergo natural (fast) drying at room temperature for subsequent STEM and TEM imaging.

3. RESULTS AND DISCUSSION

3.1. Dynamic Features. Using (single-angle) DLS analysis of P3HT/CB solutions at two different concentrations (0.4 and 10 mg/mL), Han's group[15,28] previously reported on the coexistence of two distinct relaxation modes, with the first mode assigned to single-chain species (R_h = 5.0−6.5 nm) and the second to large aggregates (R_h = 89−170 nm). Because no absorption peak at ∼607 nm was observed in the UV−vis spectrum, the aggregate species was identified to be amorphous in nature.[29] The UV−vis absorption spectra shown in Figure S2 indicate that unlike the counterpart P3HT/CB solution, the new bands of vibronic structure at longer wavelengths that are characteristic of the semicrystalline structure of P3HT/Toluene (T) solution emerge and are substantially promoted with decreased temperature, with the

DOI: 10.1021/acs.macromol.8b02619
Macromolecules 2019, 52, 332−340

general features resembling those reported elsewhere.[22,30] For the present (multiangular) DLS analysis, Figure 1 shows the field autocorrelation function, $|g^{(1)}(q,t)|$, along with the mean decay rates, $\langle\Gamma\rangle$, as a function of the scattering vector (q) for P3HT/CB solutions at four different concentrations in the dilute regime. As previously reported, the presence of two relaxation modes is evident in Figure 1a. Detailed analysis of the mode properties (see discussions below) in Figure 1b reveals, however, that while the first (fast) mode bears the usual diffusive attribute (i.e., $\langle\Gamma\rangle \sim q^2$), the second (slow) mode is clearly q-independent (i.e., $\langle\Gamma\rangle \sim q^0$) at room temperature, irrespective of the P3HT concentration. Given that the qualitative trends shown here seem to be largely unaffected by a number of experimental factors investigated shortly, the above features should be rather universal for P3HT/CB solutions.

By taking into account the effect of a slight polydispersity in particle size, we employed the following expression based on the Williams–Watt function (WWF) to fit the present DLS data:

$$|g^{(1)}(q,t)| = A_f(q)\exp[-(t/\tau_f)^{\alpha}] + A_s(q)\exp[-(t/\tau_s)^{\beta}] \quad (1)$$

where $A(q)$ denotes the relative contribution (or fraction) of the individual relaxation mode to the total scattering intensity ($A_f + A_s = 1$), and τ ($= 1/\Gamma$) is the associated decay time; α and β are the stretched exponents for the fast and slow modes, respectively, denoted by the subscripts "f" and "s". We note in passing that in the classical theories on polymer solutions $0 < \alpha$ and $\beta < 1$ for internal relaxations, with 0.5 for the Rouse model, 0.67 for the Zimm model, and 0.25 for the local reptation model.[31] Figure S3 shows the behaviors of the stretched exponent and decay time as functions of the P3HT concentration, with the fitted parameters (A_f, α, and β) gathered in Table S1. The mean value $\alpha \sim 1$ (i.e., single-exponential) is found for the fast mode and $\beta \sim 1.5$ for the slow mode. The peculiar exponent for the slow mode, $\beta \sim 1.5$, has previously been reported for weak colloidal gels as a sign of "internal stress relaxation",[32−34] although a q^1-dependence instead was often observed in this case. It can also be seen that the corresponding decay time for the slow mode τ_s increases systematically with increased polymer concentration, whereas τ_f for the fast mode remains nearly constant. The implication is that changing the P3HT concentration in the dilute regime mainly affects the properties of the aggregate species, without altering the single-chain attribute of the fast mode.

In the literature, the coexistence of the fast and slow modes has been reported for a wide variety of solution systems on the mixtures of water/organic molecules,[35−38] polyelectrolytes,[39−42] block copolymers,[43−45] and polysaccharides[46] as well as for semidilute polymer solutions[47−56] and gelation systems.[28,57−59] The slow modes, in particular, in these studies often possess distinct physical origins and apparent q-dependences, such as chain-reptation-related slow density fluctuation[31,47,48,60] and the relaxation of a transient network[28,49−52] (which bear a q^0-dependence), the translational diffusions of large temporal aggregate,[39,40] supramolecular structure,[36,37,41,43,46] nanobubble,[35,38] and dust particle[53−55] (which bear a q^2-dependence), and the internal motions of large transient cluster (which bear a q^3-dependence).[42,44,45,56−59] To clarify the physical attributes of the q^0-dependent relaxation of the slow mode for P3HT/CB solutions, we have assessed a number of experimental factors known to have influences on the properties of polymer solutions. Prior to the discussions, it is instructive to briefly examine the depolarized intensity correlation functions, $g_{VH}^{(2)}(q,t) - 1$, presented in Figure S4, which exhibit no discernible relaxation patterns that would be indicative of any pronounced anisotropy for the aggregate clusters formed in P3HT/CB solutions; namely, P3HT clusters remain in these cases isotropic (spherical) in shape.

Recently, it has been reported that without ultrasonic treatment, the 98% regioregular P3HT (which does not dissolve in CB) solutions exhibit no appreciable color changes that would be indicative of aggregate formation.[22] Moreover, the promotion of order−disorder transformation of P3HT chains via ultrasonic oscillation has been resolved by UV−vis absorption spectra.[22] These observations indicated that the ultrasonic treatment customarily used to aid the dissolution process of a conjugated polymer may have a noticeable impact on the isolated-chain and aggregate properties.

Figure S5 reveals that without sonication the slow-mode relaxation becomes even slower (without altering, however, the $\langle\Gamma\rangle \sim q^0$-dependence) while the fast mode remains basically unchanged. Moreover, Figure S2a shows that for the 10 mg/mL P3HT/CB solution the primary absorption peak at ∼455 nm, which characterizes the yellow appearance of the P3HT solution, is unaffected by the ultrasonic treatment. In summary, the DLS analysis suggests that sonication treatment, while having little influence on isolated-chain properties, can have certain impacts on the property of large aggregate species, and clearly the changes cannot be resolved by the UV−vis absorption spectra. Figure S6 shows the effect of laser-light exposure time in the DLS experiment. The results indicate no appreciable changes in τ_f and τ_s, suggesting that the isolated-chain and aggregate species remain stable over a period as long as 5 h and that possible thermal heating by laser-light absorption has a minimum impact on the DLS experiment.

One of the defining features of the slow-mode relaxation of P3HT/CB solutions is concerned with the effects of filtration, as presented in Figure 2a for a small scattering angle $\theta = 30°$;

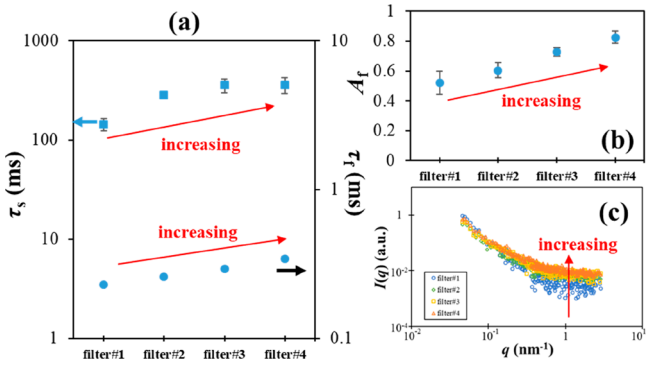

Figure 2. Effects of repeated filtrations on (a) the decay times (τ_f and τ_s) of the fast (circles) and slow (squares) modes, (b) the fraction of the fast-mode contribution at a scattering angle $\theta = 30°$, and (c) SAXS intensity profiles for the 8 mg/mL P3HT/CB solution at 25 °C.

similar results can be noted at the other scattering angles investigated (Figure S7). It should be evident that the aggregate species cannot be completely removed after repeated (four times) filtrations with a 0.45 μm PVDF filter. Interestingly, Figure 2b,c indicates that the fast-mode properties are altered, too, during the successive filtrations (e.g., R_h

DOI: 10.1021/acs.macromol.8b02619
Macromolecules 2019, 52, 332−340

changes from ~5 to ~7 nm). The contribution of the fast mode (A_f) also increases as a result of filtrations, as might be expected. For comparison, the SAXS profile reveals a major change in the high-q region reminiscent of the isolated-chain contribution, whereas the low-q profile reflecting the aggregate structure seems little altered. Importantly, the above features suggest that large aggregate species in P3HT/CB solutions are capable of re-forming right after filtration—an essential fact that would preclude possible artifacts such as dust particles as the origin of the slow mode.

Figure 3 presents the effects of system temperature; more results can be found in Figure S8. The decay times have been

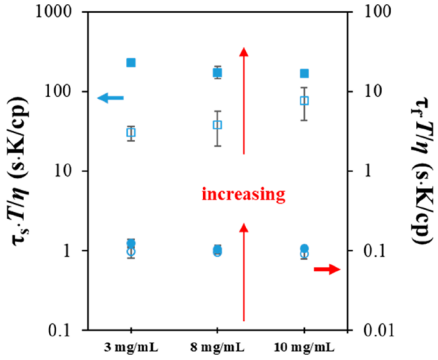

Figure 3. Effects of system temperature on the rescaled decay times of the fast (circles) and slow (squares) modes at a scattering angle θ = 30° for P3HT/CB solutions, where the solid and open symbols represent results for 15 and 25 °C, respectively.

properly rescaled so that the (trivial) effects of system temperature on the solvent viscosity (η) and chain relaxation time should not come into play. With decreased system temperature, the relaxation times of the fast and slow modes both lengthen, which is especially pronounced for the slow mode. This phenomenon may be ascribed to a progressively reduced solvent quality with decreasing system temperature, which promotes the interchain aggregates. It is worth noting, however, that the slow mode begins to exhibit a nearly single-exponential relaxation (i.e., $\beta \sim 1$; see Table S1) as well as normal diffusional behavior ($\langle\Gamma\rangle \sim q^2$; see Figure 1b) as the temperature reaches 15 °C, especially at high concentrations (c > 5 mg/mL). Along with a later structural analysis, we show that these low-temperature dynamic features are very important to understand the attributes of the aggregate cluster fostered in P3HT/CB.

Given that the static scattering analyses discussed shortly suggest that the slow mode corresponds to a microsized core−shell cluster, the decay rates determined by the WWF fits (eq 1) in Figure 1a at a small scattering angle θ = 30° are utilized to estimate the apparent diffusivities and, hence, the hydrodynamic radii ($R_{h,c}$) associated with the slow mode, as exemplified in Figure 4 for the case of 3 mg/mL P3HT/CB solution; more results can be found in Figure S9. As shown in Table 1, the $R_{h,c}$ so determined is similar to the SALS estimate of R_c (mean radius of gyration) for the core material, and the R_c/ $R_{h,c}$ ratio falls not far apart from 2.0 for the four P3HT/CB concentrations investigated. These observations suggest that the relaxation time of the slow mode correlates with the core-material diffusion. In this case, the early features (i.e., cluster re-formation after repeated filtrations and the low-temperature dynamics) suggest that the apparent *elastic* relaxation of the

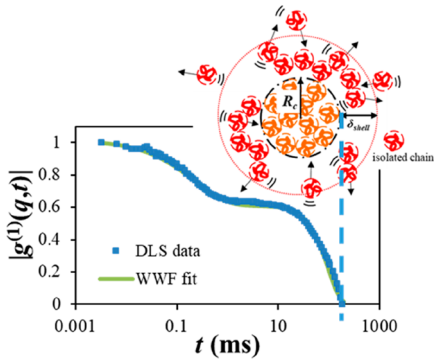

Figure 4. Field autocorrelation function, $|g^{(1)}(q,t)|$, at a scattering angle θ = 30° for the 3 mg/mL P3HT/CB solution at 25 °C. While the solid line shows the WWF fit of the DLS data that allows for the determination of an apparent hydrodynamic radius for the core material, the cartoon illustrates a possible scenario of core-and-shell (or isolated chains-cluster) reaction process that underlies the elastic response of the slow mode relaxation.

Table 1. Structural Parameters Extracted from DLS and SALS/SLS/SAXS Analyses of the P3HT/CB Solutions in This Study

		concentration (mg/mL)			
methods	parameters	3	5	8	10
DLS	$R_{h,c}$ [nm]	1429	1128	2859	4187
	$R_c/R_{h,c}$ ratio	2.53	3.25	1.47	0.99
SALS, SLS, and SAXS	radius of core (R_c) [nm]	3610	3671	4193	4162
	thickness (δ_{shell}) [nm][a]	825	740	857	771
	radius of spherical cluster (R_s) [nm]	4435	4411	5049	4933
	radius of isolated species (R_{iso}) [nm]	1.4	1.5	1.6	1.5
	$n_{isolated}$ [10^{25} cm^{-3}]	2.8	4.2	3.5	4.7
	effective radius of packing unit (R_e) [nm]	2.7	3.4	3.2	2.7
	fractal dimension (D_f)	2.66	2.65	2.61	2.81
	cutoff length (ξ) [nm]	694	759	783	866
	radius of gyration R_g_$S(q)$ [nm][b]	2167	2364	2401	2839

[a]Calculated from the relation $\delta_{shell} = R_s - R_c$. [b]Calculated from the relation R_g_$S(q) = [D_f(D_f + 1)]^{0.5}\xi$.

slow mode possibly arises from an alternating condensation/decomposition of isolated chains on the (stabilized) core, wherein the "reaction" rate is primarily dictated by the core-material diffusion. A similar process, in fact, has been observed during the sol−gel transition of pBTTT-C_{16}/CB (poly(2,5-bis(3-hexadecylthiophen-2-yl)thieno[3,2-*b*]thiophene)), of which the slow mode representing the microsized cluster evolves from an initial elastic attribute ($\langle\Gamma\rangle \sim q^0$) to a diffusive one ($\langle\Gamma\rangle \sim q^2$) at an intermediate stage of gelation when the resulting cluster seems to be "stabilized".[27] To gain deeper insight, we proceed to static scattering analyses that allow for a relatively unambiguous determination of the structural features of P3HT/CB solutions.

3.2. Static Structural Features. Multiscale scattering intensity profiles, $I(q)$, for P3HT/CB solutions utilize measurements from SALS, SLS, and SAXS techniques. The SALS and SLS profiles are vertically shifted to combine with the absolute SAXS intensity profile, and there is an excellent

DOI: 10.1021/acs.macromol.8b02619
Macromolecules 2019, 52, 332−340

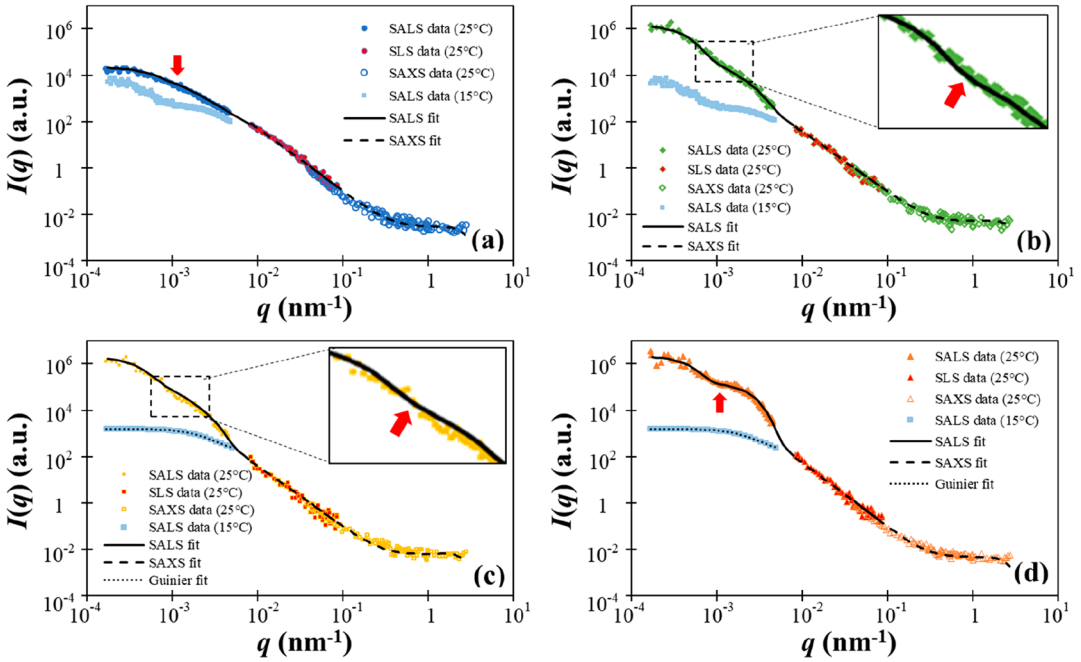

Figure 5. Vertically shifted SALS and SLS profiles combined with the absolute SAXS intensity profile (units: cm^{-1}) for (a) 3, (b) 5, (c) 8, and (d) 10 mg/mL P3HT/CB solutions at 25.0 °C. A SALS shoulder at $q = 1.2 \times 10^{-3}$ nm^{-1} is marked by an arrow in each plot. At low q (<0.01 nm^{-1}), the $I_{SALS}(q)$ data are well described by a core−shell form factor (solid lines); at higher q (for $q > 0.01$ nm^{-1}), the dashed line in each case represents the fit of $I_{SLS}(q)$ and $I_{SAXS}(q)$ data using eqs 3−5. The inset figures in (b) and (c) show the zoomed-in SALS profiles that signify the core−shell feature; for comparison, the SALS data at a lower temperature 15 °C are also shown for all four concentrations.

superposition of the SLS and SAXS data after the shift, as shown in Figure 5, with an overall q range covering length scales of about 4 orders of magnitude.

The plateau in the low-q SALS profile, $I_{SALS}(q)$, in each case clearly indicates the existence of microsized clusters in the P3HT/CB solutions investigated. An unexpected feature is, however, that the SALS profile exhibits a shoulder at $q \sim 1.2 \times 10^{-3}$ nm^{-1}, which is increasingly more pronounced with increased P3HT concentration; see the inset figures of Figure 5b,c. Similar scattering features have been reported as a manifestation of particle−particle interactions (structure factor)[61] or the formation of dumbbell[62,63] and core−shell structures.[64,65] The fitting shown in Figure 5 (solid lines) indicates that the core−shell model[65,66] (with a log-normal distribution for the radius) can be utilized to capture the SALS profile in all cases:

$$I_{\text{core-shell}}(q) = \frac{\text{scale}}{V_s}\left[3V_c(\rho_c - \rho_s)\frac{\sin(qR_c) - qR_c\cos(qR_c)}{(qR_c)^3} + 3V_s(\rho_s - \rho_{solv})\frac{\sin(qR_s) - qR_s\cos(qR_s)}{(qR_s)^3}\right]^2 \quad (2)$$

where V_s is the volume of the entire spherical cluster and V_c is the volume of the core material; R_s (= core radius + shell thickness) represents the radius of the entire spherical cluster, and R_c is the radius of the core material; ρ_c and ρ_s denote the scattering length densities of the core and shell materials, respectively, and ρ_{solv} is the scattering length density of solvent; the prefactor "scale" is related to the number density of the cluster species and, in this study, the scaling factor of the (vertically shifted) SALS data.

In the Supporting Information (see footnotes of Table S2), we describe the applications of the Rayleigh−Debye−Gans theory[67,68] along with the measured (concentration-dependent) refractive indices for the P3HT/CB solutions to estimate $\rho_c - \rho_s$ and $\rho_s - \rho_{solvent}$ in eq 2 for the present SALS experiment. To ascertain the validity of the core−shell model, we have also performed SALS measurements based on a longer wavelength (i.e., λ_0 = 785 nm; Omicrometer, LuxX 785, Germany) to create a different contrast between the core−shell cluster and the solvent medium (Figure S11), as often achieved by varying the solvent medium or its composition.[69,70] The good agreement between the results shown in Table 1 and Table S2 for the geometrical features so determined confirms the core−shell form factor fits for the SALS data reported herein.

Additionally, we have evaluated the possibility of two distinct cluster species accounting for the double plateaus in the SALS profile, and the model fits are shown in Figure S10 with the estimated cluster sizes being about 800 and 3000 nm (see Table S2). Clearly, two distinct cluster species falling in this size range should be readily detectable by the DLS analysis, inconsistent with the present observations. Besides, although the peculiar SALS profiles noticed here resemble ones having a hierarchical structure, the separation of the two plateaus seems too narrow to rationalize that this could be the case.[27,71] Finally, the impact of cluster−cluster interaction—or interparticle structure factor—that might give rise to a similar peak in the SALS profile is precluded because this would correspond to a characteristic diameter of $1/q_{peak} \approx 800$ nm (q_{peak} being the location of local maximum) within the equivalent hard-sphere (EHS) potential, which falls substantially below the mean core diameter of P3HT clusters (~8 μm in Table 1). Besides, the peak position exhibits no systematic shifts toward larger q with increased P3HT concentration or

DOI: 10.1021/acs.macromol.8b02619
Macromolecules 2019, 52, 332−340

becomes more prominent at a lower temperature (15 °C) that would signify the effects of cluster−cluster interactions. In fact, the q^0-dependent (elastic) response of the DLS relaxation for the cluster species indicated a more intimate interaction between the two species involved, such as the state of loosely bonded core and shell materials that undergo the transition as remarked earlier.

At higher q, the SLS data reflect the interior structure of the cluster species. The SLS profile along with the low-q part of SAXS profile (q < 0.1 nm^{-1}) is indicative of a mass fractal structure and, therefore, may be described by the product of a form factor and structure factor. Without knowing the true attributes of the packing units, we consider both the form factors for spherical particle and Gaussian chain, along with a rather general (mass fractal) structure factor $S(q)$, to describe the contribution from the packing P3HT chains or small aggregates. The results based on the Gaussian-chain model ($P_{chain}(q)$) are shown by the dashed lines in Figure 5; for comparison, the model fits that utilize the spherical-particle form factor are presented in Figure S10 and Table S2. The remaining high-q part of SAXS profile, which falls mainly in the Guinier region, is fitted with the same form factor (Gaussian chain or spherical particle) along with a log-normal distribution (PDI ∼ 1.3) for the radius to determine the mean radius of the isolated species (i.e., single chain or small aggregate). The full set of formulas employed in the fits is given below, with the structural parameters gathered in Table 1:

$$I_{SAXS}(q) \sim P_{chain}(q)S(q) + n_{isolated}\Delta\rho_{isolated}{}^2V_{isolated}{}^2P_{chain}(q) \quad (3)$$

$$P_{chain}(q) = 2\left(\frac{\exp[-(qR_{iso})^2] + (qR_{iso})^2 - 1}{(qR_{iso})^4}\right) \quad (4)$$

$$S(q) = 1 + \frac{D_f\Gamma(D_f - 1)\sin(D_f - 1)\tan^{-1}(q\xi)}{(qR_e)^{D_f}[1 + (q\xi)^{-2}]^{(D_f-1)/2}} \quad (5)$$

In eqs 3−5, R_{iso} denotes the radius of gyration of the isolated species, D_f represents the fractal dimension of the cluster interior, ξ is the cutoff length marking the boundary of an aggregate cluster and thus should bear a magnitude comparable with the mean size of a P3HT cluster, and R_e reflects the dimension of the packing unit. The second term on the right side of eq 3, which takes advantage of the absolute SAXS intensity, represents the contribution of the isolated species, where $n_{isolated}$ denotes the number density of the isolated species, $\Delta\rho_{isolated}$ is the scattering length density contrast between P3HT and CB, and $V_{isolated}$ is the volume of an isolated species. The scattering length densities (SLD) of P3HT and CB are evaluated using the NIST SLD calculator to be $\rho_{P3HT} = 0.68 \times 10^{-6}$ Å^{-2} and $\rho_{CB} = 1.83 \times 10^{-6}$ Å^{-2} for the SAXS experiment.

Along with the previous DLS analysis, the P3HT cluster is suggested to be constituted by a condensed core material (R_c ∼ 4 μm) being encompassed by a loose corona material (∼700 nm in thickness). From the results gathered in Table 1, it can be seen that there is a reasonable agreement between DLS and SALS analyses on the core radius, as mentioned earlier. Several features should be further noted. First, the fractal dimension in Table 1 indicates a slightly increased compactness of aggregate interior only at a high P3HT concentration of 10 mg/mL. Second, the mean sizes of fractal aggregates as calculated from ξ (i.e., R_g_$S(q)$) are in reasonable agreement with the results from the (core−shell) form factor analysis (i.e., R_s). Third, the size of the packing unit determined from the structure factor $S(q)$ (R_e ∼ 3 nm) is not much different from that evaluated from the form factor for the isolated species (R_{iso} ∼ 1.5 and ∼1.1 nm for Gaussian-chain and spherical-particle form factors, respectively), suggesting that they might represent the same or similar species. Finally, the number density of the isolated species, $n_{isolated}$, quickly reaches a nearly constant value (∼4 × 10^{25} cm^{-3}) at 5 mg/mL, suggesting that the two coexistent species (i.e., isolated chain/aggregate and cluster) in P3HT/CB solutions have then reached the analogous critical micelle concentration (cmc).

We mentioned earlier that the core−shell structure and anomalous slow-mode relaxation associated with P3HT/CB solutions disappear at a low temperature (15 °C) and high concentration (c > 5 mg/mL), as can be seen from the SALS profiles shown in Figure 5c,d, when one has a homogeneous (and apparently smaller) cluster that exhibits the normal diffusional behavior (i.e., q^2-dependence). In this case, the shell material appears to have been substantially condensed to be indistinguishable from the core material. In fact, the dynamic equilibrium of isolated-chain and aggregate species resolved in the DLS analysis has previously been reported for dilute P3HT/THF solutions, as the low- and high-molecular-weight fractions of P3HT were effectively removed during the sample preparation.[21,23] This study shows that under usual sample preparation conditions P3HT/CB solutions exhibit a similar coexistence of two distinct species, only that their peculiar interactions further add to the richness of admissible aggregation state for a commonplace conjugated polymer like P3HT.

Figure 6 presents the STEM and TEM morphologies of drop-casting thin film produced from the 10 mg/mL P3HT/CB solution. A fast drying of the thin-film sample before the image was taken helps preserve the aggregate features in solution.[72] The results clearly confirm the spherical feature as well as the mean size of P3HT clusters fostered in CB, as resolved in prior dynamic/static scattering analyses. For (annealed) thin films spin-coated from P3HT/CB solutions, Xue et al.[15] have previously reported on similar sphere-like aggregates in AFM imaging. Although the darker region of the cluster interior in Figure 6b could be indicative of the core material, to clearly distinguish between the core and shell materials seems unlikely at this stage. It is worth noting that similar core−shell structures seen in TEM images have been reported for the aggregate species formed by polyelectrolyte molecules,[41] and the shell material was suggested to represent loosely packed chains with dangling ends under the influence of electrostatic repulsions. An important difference from the present finding is, however, that the slow mode reported therein exhibited the normal diffusional motion, and therefore,

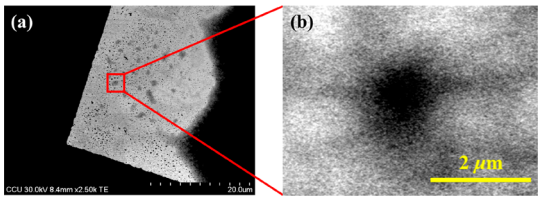

Figure 6. (a) STEM and (b) TEM morphologies of drop-casting thin film produced from the 10 mg/mL P3HT/CB solution at 25.0 °C.

DOI: 10.1021/acs.macromol.8b02619
Macromolecules 2019, 52, 332−340

the core−shell polyelectrolyte cluster likely was formed at one time and remained intact over the DLS resolution times.

In practical applications with OTFTs[73] and OPVs,[74] the thin film cast from P3HT/T solutions has been reported to yield high electrical performance, especially after the post-treatment of thermal annealing. The results shown in Figure S12 for the solution-state ac conductivity reveal, however, that the 10 mg/mL P3HT/CB solutions produce much higher values than their P3HT/T counterparts, while the core−shell structure incubated under the P3HT/CB solution at 25.0 °C leads to a slightly higher value than its companion at 15.0 °C which produces only the usual spherical clusters. Considering that reducing the system temperature typically results in a more compact aggregate structure and, hence, higher electrical conductivity, as can be noted for the 10 mg/mL P3HT/T solutions, the increase in ac conductivity associated with the core−shell structure in the P3HT/CB solution at 25.0 °C has an interesting implication and is worth pursuing in future applications.

4. CONCLUSION

We report on results from detailed dynamic and structural analyses of a representative series of dilute P3HT/CB solutions, revealing the coexistence and dynamic equilibrium of isolated chains ($R_g \sim 1.5$ nm) and microsized clusters ($R_g \sim 4$ μm). Independent of a number of experimental factors investigated herein, the cluster species is shown to possess universal dynamic (nondiffusive) and structural (core−shell) features that, together, went previously unnoticed for P3HT solutions in particular and homopolymer solutions in general. Among the defining features is that the microsized cluster may be re-formed spontaneously after repeated filtrations. Accordingly, the core−shell cluster is suggested to be formed during the dynamic equilibrium process wherein the isolated chains undergo condensation/decomposition on the (stabilized) core material, leading to an apparent (elastic) q^0-dependence of the slow-mode relaxation whose rate is set by the core-material diffusion. Only at a low temperature (15 °C) and high concentration ($c > 5$ mg/mL) does the shell material become indistinguishable from the core material, when one has a homogeneous and fairly condensed cluster that exhibits the normal diffusional behavior (q^2-dependence). In view of highly diverse performances of P3HT-based device in early reports, the experimental factors examined herein by the DLS analysis clearly reveal their impact on the aggregate cluster and isolated chain properties. It is also significant to observe that the representative 10 mg/mL P3HT/CB solutions possess substantially higher ac conductivity than their P3HT/T counterparts, wherein the core−shell cluster incubated under the P3HT/CB solution at 25.0 °C appears to play an important role. Overall, the present findings provide new insight into the mechanistic aspects and precise controls of the morphological features of P3HT in solution for future applications with polymer-based electronic devices.

■ ASSOCIATED CONTENT

Supporting Information

The Supporting Information is available free of charge on the ACS Publications website at DOI: 10.1021/acs.macromol.8b02619.

Intrinsic viscosity analysis of P3HT/CB solutions, UV−vis absorption spectra of P3HT/CB and P3HT/T solutions, a full collection of DLS data that show the effects of concentration, sonication, laser-light exposure time, filtration, and system temperature on the stretched exponents, decay times, and fraction of the fast-mode contribution to total scattering intensity, geometrical features of the core−shell cluster from different SALS experiments and model fits, ac conductivities of P3HT/CB and P3HT/T solutions (PDF)

■ AUTHOR INFORMATION

Corresponding Author

*E-mail: chmcch@ccu.edu.tw (C.C.H.).

ORCID

Chi-Chung Hua: 0000-0003-3398-2576

Notes

The authors declare no competing financial interest.

■ ACKNOWLEDGMENTS

This research was supported by the Ministry of Science and Technology of ROC (MOST 107-2221-E-194-006). We acknowledge the NSRRC of ROC for providing beamtimes and facilitating the SAXS experiments.

■ REFERENCES

(1) Chiang, C. K.; Fincher, C. R.; Park, Y. W.; Heeger, A. J.; Shirakawa, H.; Louis, E. J.; Gau, S. C.; MacDiarmid, A. G. Electrical Conductivity in Doped Polyacetylene. *Phys. Rev. Lett.* **1977**, *39*, 1098−1101.

(2) Shirakawa, H.; Louis, E. J.; MacDiarmid, A. G.; Chiang, C. K.; Heeger, A. J. Synthesis of Electrically Conducting Organic Polymers: Halogen Derivatives of Polyacetylene, $(CH)_x$. *J. Chem. Soc., Chem. Commun.* **1977**, 578−580.

(3) Skotheim, T. A.; Reynolds, J. *Conjugated Polymers: Processing and Applications*; CRC Press: Boca Raton, FL, 2006.

(4) Ludwigs, S. *P3HT Revisited-from Molecular Scale to Solar Cell Devices*; Springer: New York, 2015.

(5) Skotheim, T. A.; Reynolds, J. *Conjugated Polymers: Theory, Synthesis, Properties, and Characterization*; CRC Press: Boca Raton, FL, 2006.

(6) Scharsich, C.; Lohwasser, R. H.; Sommer, M.; Asawapirom, U.; Scherf, U.; Thelakkat, M.; Neher, D.; Köhler, A. Control of Aggregate Formation in Poly(3-hexylthiophene) by Solvent, Molecular Weight, and Synthetic Method. *J. Polym. Sci., Part B: Polym. Phys.* **2012**, *50*, 442−453.

(7) Aiyar, A. R.; Hong, J.-I.; Izumi, J.; Choi, D.; Kleinhenz, N.; Reichmanis, E. Ultrasound-Induced Ordering in Poly(3-hexylthiophene): Role of Molecular and Process Parameters on Morphology and Charge Transport. *ACS Appl. Mater. Interfaces* **2013**, *5*, 2368−2377.

(8) Zen, A.; Pflaum, J.; Hirschmann, S.; Zhuang, W.; Jaiser, F.; Asawapirom, U.; Rabe, J. P.; Scherf, U.; Neher, D. Effect of Molecular Weight and Annealing of Poly(3-hexylthiophene)s on the Performance of Organic Field-Effect Transistors. *Adv. Funct. Mater.* **2004**, *14*, 757−764.

(9) Noriega, R.; Rivnay, J.; Vandewal, K.; Koch, F. P. V.; Stingelin, N.; Smith, P.; Toney, M. F.; Salleo, A. A General Relationship between Disorder, Aggregation and Charge Transport in Conjugated Polymers. *Nat. Mater.* **2013**, *12*, 1038.

(10) Herrmann, D.; Niesar, S.; Scharsich, C.; Köhler, A.; Stutzmann, M.; Riedle, E. Role of Structural Order and Excess Energy on Ultrafast Free Charge Generation in Hybrid Polythiophene/Si Photovoltaics Probed in Real Time by Near-Infrared Broadband Transient Absorption. *J. Am. Chem. Soc.* **2011**, *133*, 18220−18233.

(11) Schwartz, B. J. Conjugated Polymers as Molecular Materials: How Chain Conformation and Film Morphology Influence Energy

DOI: 10.1021/acs.macromol.8b02619
Macromolecules 2019, 52, 332−340

Transfer and Interchain Interactions. *Annu. Rev. Phys. Chem.* **2003**, *54*, 141−172.
(12) de Oliveira, E. F.; Lavarda, F. C. Structure of P3HT in the Solid State. *J. Polym. Sci., Part B: Polym. Phys.* **2013**, *51*, 1350−1354.
(13) Botiz, I.; Stingelin, N. Influence of Molecular Conformations and Microstructure on the Optoelectronic Properties of Conjugated Polymers. *Materials* **2014**, *7*, 2273.
(14) Dierckx, W.; Oosterbaan, W. D.; Bolsee, J.-C.; Maes, W.; Vanderzande, D.; Manca, J. Poly(3-alkylthiophene) Nanofibers for Optoelectronic Devices. *J. Mater. Chem. C* **2014**, *2*, 5730−5746.
(15) Xue, L.; Yu, X.; Han, Y. Different Structures and Crystallinities of Poly(3-hexylthiophene) Films Prepared from Aged Solutions. *Colloids Surf., A* **2011**, *380*, 334−340.
(16) Xue, L.; Gao, X.; Zhao, K.; Liu, J.; Yu, X.; Han, Y. The Formation of Different Structures of Poly(3-hexylthiophene) Film on a Patterned Substrate by Dip Coating from Aged Solution. *Nanotechnology* **2010**, *21*, 145303.
(17) Newbloom, G. M.; Kim, F. S.; Jenekhe, S. A.; Pozzo, D. C. Mesoscale Morphology and Charge Transport in Colloidal Networks of Poly(3-hexylthiophene). *Macromolecules* **2011**, *44*, 3801−3809.
(18) Zhao, K.; Yu, X.; Li, R.; Amassian, A.; Han, Y. Solvent-Dependent Self-Assembly and Ordering in Slow-Drying Drop-Cast Conjugated Polymer Films. *J. Mater. Chem. C* **2015**, *3*, 9842−9848.
(19) Park, Y. D.; Lee, H. S.; Choi, Y. J.; Kwak, D.; Cho, J. H.; Lee, S.; Cho, K. Solubility-Induced Ordered Polythiophene Precursors for High-Performance Organic Thin-Film Transistors. *Adv. Funct. Mater.* **2009**, *19*, 1200−1206.
(20) Yang, H.; Shin, T. J.; Yang, L.; Cho, K.; Ryu, C. Y.; Bao, Z. Effect of Mesoscale Crystalline Structure on the Field-Effect Mobility of Regioregular Poly(3-hexyl thiophene) in Thin-Film Transistors. *Adv. Funct. Mater.* **2005**, *15*, 671−676.
(21) Huang, Y.; Cheng, H.; Han, C. C. Unimer−Aggregate Equilibrium to Large Scale Association of Regioregular Poly(3-hexylthiophene) in THF Solution. *Macromolecules* **2011**, *44*, 5020−5026.
(22) Zhao, K.; Xue, L.; Liu, J.; Gao, X.; Wu, S.; Han, Y.; Geng, Y. A New Method to Improve Poly(3-hexyl thiophene) (P3HT) Crystalline Behavior: Decreasing Chains Entanglement to Promote Order−Disorder Transformation in Solution. *Langmuir* **2010**, *26*, 471−477.
(23) Huang, Y.; Cheng, H.; Han, C. C. Temperature Induced Structure Evolution of Regioregular Poly(3-hexylthiophene) in Dilute Solution and its Influence on Thin Film Morphology. *Macromolecules* **2010**, *43*, 10031−10037.
(24) Wen, Y. H.; Lin, P. C.; Hua, C. C.; Chen, S. A. Dynamic Structure Factor for Large Aggregate Clusters with Internal Motions: A Self-Consistent Light-Scattering Study on Conjugated Polymer Solutions. *J. Phys. Chem. B* **2011**, *115*, 14369−14380.
(25) Guo, R. H.; Hsu, C. H.; Hua, C. C.; Chen, S. A. Colloidal Aggregate and Gel Incubated by Amorphous Conjugated Polymer in Hybrid-Solvent Medium. *J. Phys. Chem. B* **2015**, *119*, 3320−3331.
(26) Yi, H. L.; Wu, C. H.; Wang, C. I.; Hua, C. C. Solvent-Regulated Mesoscale Aggregation Properties of Dilute pBTTT-C_{14} Solutions. *Macromolecules* **2017**, *50*, 5498−5509.
(27) Yi, H.-L.; Hua, C.-C. PBTTT-C_{16} Sol-Gel Transition by Hierarchical Colloidal Bridging. *Soft Matter* **2018**, *14*, 1270−1280.
(28) Liu, J.; Shao, S.; Wang, H.; Zhao, K.; Xue, L.; Gao, X.; Xie, Z.; Han, Y. The Mechanisms for Introduction of *n*-dodecylthiol to Modify the P3HT/PCBM Morphology. *Org. Electron.* **2010**, *11*, 775−783.
(29) Clark, J.; Silva, C.; Friend, R. H.; Spano, F. C. Role of Intermolecular Coupling in the Photophysics of Disordered Organic Semiconductors: Aggregate Emission in Regioregular Polythiophene. *Phys. Rev. Lett.* **2007**, *98*, 206406.
(30) Rughooputh, S.; Hotta, S.; Heeger, A.; Wudl, F. Chromism of Soluble Polythienylenes. *J. Polym. Sci., Part B: Polym. Phys.* **1987**, *25*, 1071−1078.
(31) Doi, M.; Edwards, S. F. *The Theory of Polymer Dynamics*; Clarendon Press: New York, 1988.
(32) Mohraz, A.; Solomon, M. J. Gelation and Internal Dynamics of Colloidal Rod Aggregates. *J. Colloid Interface Sci.* **2006**, *300*, 155−162.
(33) Solomon, M. J.; Varadan, P. Dynamic Structure of Thermoreversible Colloidal Gels of Adhesive Spheres. *Phys. Rev. E: Stat. Phys., Plasmas, Fluids, Relat. Interdiscip. Top.* **2001**, *63*, 051402.
(34) Cipelletti, L.; Manley, S.; Ball, R. C.; Weitz, D. A. Universal Aging Features in the Restructuring of Fractal Colloidal Gels. *Phys. Rev. Lett.* **2000**, *84*, 2275−2278.
(35) Jin, F.; Ye, J.; Hong, L.; Lam, H.; Wu, C. Slow Relaxation Mode in Mixtures of Water and Organic Molecules: Supramolecular Structures or Nanobubbles? *J. Phys. Chem. B* **2007**, *111*, 2255−2261.
(36) González-Gaitano, G.; Rodríguez, P.; Isasi, J. R.; Fuentes, M.; Tardajos, G.; Sánchez, M. The Aggregation of Cyclodextrins as Studied by Photon Correlation Spectroscopy. *J. Inclusion Phenom. Mol. Recognit. Chem.* **2002**, *44*, 101−105.
(37) Sedlák, M. Large-Scale Supramolecular Structure in Solutions of Low Molar Mass Compounds and Mixtures of Liquids: I. Light Scattering Characterization. *J. Phys. Chem. B* **2006**, *110*, 4329−4338.
(38) Jin, F.; Li, J.; Ye, X.; Wu, C. Effects of pH and Ionic Strength on the Stability of Nanobubbles in Aqueous Solutions of α-cyclodextrin. *J. Phys. Chem. B* **2007**, *111*, 11745−11749.
(39) Zhou, K.; Li, J.; Lu, Y.; Zhang, G.; Xie, Z.; Wu, C. Re-Examination of Dynamics of Polyeletrolytes in Salt-Free Dilute Solutions by Designing and Using a Novel Neutral−Charged−Neutral Reversible Polymer. *Macromolecules* **2009**, *42*, 7146−7154.
(40) Cao, Z.; Zhang, G. Insight into Dynamics of Polyelectrolyte Chains in Salt-Free Solutions by Laser Light Scattering and Analytical Ultracentrifugation. *Polymer* **2014**, *55*, 6789−6794.
(41) Korchagina, E. V.; Philippova, O. E. Multichain Aggregates in Dilute Solutions of Associating Polyelectrolyte Keeping a Constant Size at the Increase in the Chain Length of Individual Macromolecules. *Biomacromolecules* **2010**, *11*, 3457−3466.
(42) Peitzsch, R. M.; Burt, M. J.; Reed, W. F. Evidence of Partial Draining for Linear Polyelectrolytes; Heparin, Chondroitin 6-Sulfate, and Poly(styrene sulfonate). *Macromolecules* **1992**, *25*, 806−815.
(43) Koňák, Č.; Helmstedt, M.; Bansil, R. Dynamics in Solutions of Associating Statistical Copolymers. *Macromolecules* **1997**, *30*, 4342−4346.
(44) Ngai, T.; Wu, C. Effect of Cross-Linking on Dynamics of Semidilute Copolymer Solutions: Poly(methyl methacrylate-*co*-7-acryloyloxy-4-methylcoumarin) in Chloroform. *Macromolecules* **2003**, *36*, 848−854.
(45) Yuan, G.; Wang, X.; Han, C. C.; Wu, C. Reexamination of Slow Dynamics in Semidilute Solutions: From Correlated Concentration Fluctuation to Collective Diffusion. *Macromolecules* **2006**, *39*, 3642−3647.
(46) Zhang, Y.; Li, S.; Zhang, L. Aggregation Behavior of Triple Helical Polysaccharide with Low Molecular Weight in Diluted Aqueous Solution. *J. Phys. Chem. B* **2010**, *114*, 4945−4954.
(47) Wang, J.; Wu, C. Reexamination of the Origin of Slow Relaxation in Semidilute Polymer Solutions—Reptation Related or Not? *Macromolecules* **2016**, *49*, 3184−3191.
(48) Li, J.; Li, W.; Huo, H.; Luo, S.; Wu, C. Reexamination of the Slow Mode in Semidilute Polymer Solutions: The Effect of Solvent Quality. *Macromolecules* **2008**, *41*, 901−911.
(49) Yuan, G.; Wang, X.; Han, C. C.; Wu, C. Reexamination of Slow Dynamics in Semidilute Solutions: Temperature and Salt Effects on Semidilute Poly(*N*-isopropylacrylamide) Aqueous Solutions. *Macromolecules* **2006**, *39*, 6207−6209.
(50) Li, J.-f.; Lu, Y.-j.; Zhang, G.-z.; Li, W.; Wu, C. A Slow Relaxation Mode of Polymer Chains in a Semidilute Solution. *Chin. J. Polym. Sci.* **2008**, *26*, 465−473.
(51) Ewen, B.; Richter, D.; Farago, B.; Stühn, B. Neutron Spin Echo Investigations on the Segmental Dynamics in Semidilute Polymer Solutions under θ- and Good Solvent Conditions. *J. Non-Cryst. Solids* **1994**, *172-174*, 1023−1027.
(52) Adam, M.; Delsanti, M. Dynamical Behavior of Semidilute Polymer Solutions in a θ Solvent: Quasi-Elastic Light Scattering Experiments. *Macromolecules* **1985**, *18*, 1760−1770.

DOI: 10.1021/acs.macromol.8b02619
Macromolecules 2019, 52, 332−340

(53) Adam, M.; Delsanti, M. Dynamical Properties of Polymer Solutions in Good Solvent by Rayleigh Scattering Experiments. *Macromolecules* **1977**, *10*, 1229−1237.
(54) Brown, W.; Stepanek, P. Distribution of Relaxation Times from Dynamic Light Scattering on Semidilute Solutions: Polystyrene in Ethyl Acetate as a Function of Temperature from Good to θ Conditions. *Macromolecules* **1988**, *21*, 1791−1798.
(55) Amis, E. J.; Han, C. C. Cooperative and Self-Diffusion of Polymers in Semidilute Solutions by Dynamic Light Scattering. *Polymer* **1982**, *23*, 1403−1406.
(56) Chu, B.; Nose, T. Static and Dynamical Properties of Polystyrene in *trans*-Decalin. 4. Osmotic Compressibility, Characteristic Lengths, and Internal and Pseudogel Motions in the Semidilute Regime. *Macromolecules* **1980**, *13*, 122−132.
(57) Ngai, T.; Wu, C.; Chen, Y. Effects of Temperature and Swelling on Chain Dynamics During the Sol−Gel Transition. *Macromolecules* **2004**, *37*, 987−993.
(58) Ngai, T.; Wu, C.; Chen, Y. Origins of the Speckles and Slow Dynamics of Polymer Gels. *J. Phys. Chem. B* **2004**, *108*, 5532−5540.
(59) Wu, C.; Ngai, T. Reexamination of Slow Relaxation of Polymer Chains in Sol−Gel Transition. *Polymer* **2004**, *45*, 1739−1742.
(60) de Gennes, P. G. *Scaling Concepts in Polymer Physics*; Cornell University Press: Ithaca, NY, 1979.
(61) Fernandes, N. J.; Akbarzadeh, J.; Peterlik, H.; Giannelis, E. P. Synthesis and Properties of Highly Dispersed Ionic Silica−Poly(ethylene oxide) Nanohybrids. *ACS Nano* **2013**, *7*, 1265−1271.
(62) Shtykova, E. V.; Malyutin, A.; Dyke, J.; Stein, B.; Konarev, P. V.; Dragnea, B.; Svergun, D. I.; Bronstein, L. M. Hydrophilization of Magnetic Nanoparticles with Modified Alternating Copolymers. Part 2: Behavior in Solution. *J. Phys. Chem. C* **2010**, *114*, 21908−21913.
(63) Shtykova, E. V.; Huang, X.; Remmes, N.; Baxter, D.; Stein, B.; Dragnea, B.; Svergun, D. I.; Bronstein, L. M. Structure and Properties of Iron Oxide Nanoparticles Encapsulated by Phospholipids with Poly(ethylene glycol) Tails. *J. Phys. Chem. C* **2007**, *111*, 18078−18086.
(64) Grünewald, T. A.; Lassenberger, A.; van Oostrum, P. D. J.; Rennhofer, H.; Zirbs, R.; Capone, B.; Vonderhaid, I.; Amenitsch, H.; Lichtenegger, H. C.; Reimhult, E. Core−Shell Structure of Monodisperse Poly(ethylene glycol)-Grafted Iron Oxide Nanoparticles Studied by Small-Angle X-Ray Scattering. *Chem. Mater.* **2015**, *27*, 4763−4771.
(65) Chu, B.; Wu, G.; Schneider, D. K. A Scattering Study on Intermicellar Interactions and Structures of Polymeric Micelles. *J. Polym. Sci., Part B: Polym. Phys.* **1994**, *32*, 2605−2614.
(66) Guinier, A.; Fournet, G. *Small-Angle Scattering of X-Rays*; Wiley: New York, 1955.
(67) Casperson, L. W.; Yeh, C. Rayleigh-Debye Scattering with Focused Laser Beams. *Appl. Opt.* **1978**, *17*, 1637−1643.
(68) LS Instruments AG; https://Lsinstruments.Ch/En/ (accessed December 6, 2018).
(69) Voudouris, P.; Choi, J.; Dong, H.; Bockstaller, M. R.; Matyjaszewski, K.; Fytas, G. Effect of Shell Architecture on the Static and Dynamic Properties of Polymer-Coated Particles in Solution. *Macromolecules* **2009**, *42*, 2721−2728.
(70) Suresh, K. I.; Bartsch, E. Effect of Seed Characteristics on Morphology Development in Poly(*n*-butyl acrylate)-Poly(*n*-butyl methacrylate) Core-Shell Dispersions. *J. Appl. Polym. Sci.* **2013**, *127*, 208−216.
(71) Koga, T.; Hashimoto, T.; Takenaka, M.; Aizawa, K.; Amino, N.; Nakamura, M.; Yamaguchi, D.; Koizumi, S. New Insight into Hierarchical Structures of Carbon Black Dispersed in Polymer Matrices: A Combined Small-Angle Scattering Study. *Macromolecules* **2008**, *41*, 453−464.
(72) Zhao, H.; Chen, Q.; Hong, L.; Zhao, L.; Wang, J.; Wu, C. What Morphologies Do We Want? − TEM Images from Dilute Diblock Copolymer Solutions. *Macromol. Chem. Phys.* **2011**, *212*, 663−672.
(73) Bao, Z.; Dodabalapur, A.; Lovinger, A. J. Soluble and Processable Regioregular Poly(3-hexylthiophene) for Thin Film Field-Effect Transistor Applications with High Mobility. *Appl. Phys. Lett.* **1996**, *69*, 4108−4110.
(74) Oh, J. Y.; Shin, M.; Lee, T. I.; Jang, W. S.; Min, Y.; Myoung, J.-M.; Baik, H. K.; Jeong, U. Self-Seeded Growth of Poly(3-hexylthiophene) (P3HT) Nanofibrils by a Cycle of Cooling and Heating in Solutions. *Macromolecules* **2012**, *45*, 7504−7513.

DOI: 10.1021/acs.macromol.8b02619
Macromolecules 2019, 52, 332−340